Received 8 September; accepted 13 November 1992.

1. Hoyle, F. in *Paris Symp. Radio Astronomy, IAU Symp.* No 9 (ed. Bracewell, R.) 529–532 (1959).
2. Sandage, A. R. *Astrophys. J.* **133,** 355–392 (1961).
3. Sandage, A. R. *Astrophys. J.* **173,** 485–499 (1973).
4. Sandage, A. R. *A. Rev. Astr. Astrophys.* **26,** 561–630 (1988).
5. Miley, G. K. *Mon. Not. R. astr. Soc.* **152,** 477–489 (1970).
6. Legg T. H. *Nature* **226,** 65–67 (1970).
7. Wardle, J. F. C. & Miley, G. K. *Astr. Astrophys.* **30,** 305–315 (1974).
8. Kapahi, V. K. in *Observational Cosmology, IAU Symp.* No. 124 (ed. Hewitt, A. Burbidge, G. & Fang, L. Z.) 251–265 (1987).
9. Oort, M. J. A., Katgert, P., Steeman, F. W. M. & Windhorst, R. A. *Astr. Astrophys.* **179,** 41–59 (1987).
10. Singal, A. K. *Mon. Not. R. astr. Soc.* **233,** 87–113 (1988).
11. Kapahi, V. K. *Astr. J.* **97,** 1–9 (1989).
12. Gopal-Krishna & Wiita, P. J. *Astrophys. J.* **373,** 325–335.
13. Subramanian, K. & Swarup, G. *Mon. Not. R. astr. Soc.* **247,** 237–243.
14. Cohen, M. H. in *BL Lac Objects* (ed. Maraschi, L., Maccacaro, T. & Ulrich, M.-H.) 13–21 (1989).
15. Pearson, T. *J. in Parsec Scale Radio Jets* (ed. Zensus, A.) 1–12 (1990).
16. Pearson, T. J. & Readhead, A. C. S. *Astrophys. J.* **328,** 114–142 (1988).
17. Wilkinson, P. N., Polatidis, A., Readhead, A. C. S., Xu, W. & Pearson, T. J. in *Sub Arc Second Radio Astronomy* (ed. Davis, R. J.) (Cambridge Univ. Press, in the press).
18. Gurvits, L. I. *et al. Astr. Astrophys.* **260,** 82–88 (1992).
19. Ekhart, A. *et al. Astr. Astrophys. Suppl. Soc.* **67,** 121–146 (1987).
20. Wehrele, A. *et al. Astrophys. J.* **391,** 589–607 (1992).
21. Kellermann, K. I., Sramek, R., Schmidt, M. & Shaffer, D. B. *Astr. J.* **98,** 1195–1207 (1989).
22. Fanaroff, B. L. & Riley, J. M. *Mon. Not. R. astr. Soc.* **167,** 31p–35p (1974).

ACKNOWLEDGEMENTS. The NRAO is operated by Associated Universities, Inc., under cooperative agreement with the NSF.

Pulsed X-rays from the Vela pulsar

H. Ögelman*†, J. P. Finley* & H. U. Zimmermann†

* Department of Physics, University of Wisconsin-Madison, 1150 University Avenue, Madison, Wisconsin 53706, USA
† Max-Planck-Institut für Extraterrestrische Physik, D-8046 Garching, Germany

THE Vela pulsar, PSR0833-45, is a young (10^4 yr) nearby neutron star emitting pulsed radiation in radio, optical and γ-ray bands[1–5]. Soft X-ray imaging by the Einstein[6] and Exosat[7] observatories has revealed a point-like source, at the position of the pulsar, embedded in a compact nebula ~2 arcmin in diameter, but the search for pulsed X-ray emission has proved difficult. There were claims in 1973 of a positive detection[8,9] but subsequent observations have failed to confirm them[6,10]. Here we report an unambiguous detection, by means of the Rosat satellite[11], of pulsed X-ray emission from the Vela pulsar, and thus put this long-standing enigma to rest. The pulsed signal is soft, appearing mainly at energies <1 keV. The Rosat observations resolve the two sources of emission, and show that the point-like emission centred on the pulsar is soft, whereas the emission from the compact nebula is hard. Despite the common prejudice that it is the archetypal young pulsar embedded in a supernova remnant, these observations show that Vela more closely resembles older (10^5 yr) pulsars.

With their strong magnetic fields and short periods, pulsars are expected to generate high voltages and accelerate high-energy electrons and positrons in their magnetospheres which in turn should radiate in X- and γ-rays. Furthermore, the hot surface of a cooling neutron star should be a source of soft X-rays. Up to the present, only a handful of pulsars have been observed to emit energetic photons. It is clearly of interest to observe these objects in the X-ray band and study their spectral and timing characteristics. The Vela pulsar is particularly interesting in that it is one of the closest 'active' neutron stars which, considering its 10^4-yr age and 89-ms period, should emit X-rays both from magnetospheric processes and initial cooling.

Rosat observed the Vela pulsar during two sets of pointings about 8 months apart, 1991 April 22.0–23.9 and 1991 December 4.7–19.8, with effective exposure times of 13,900 s and 18,500 s respectively. For the timing analysis, we selected all the photons within a radius of 42′ centred on the pulsar yielding 48,167 and 61,742 photons with consistent count rates of 3.4 s^{-1}. Recognized software errors in the timing were corrected in the analysis. The photon arrival times of the selected events were corrected to the Solar System barycentre in the barycentric dynamical time unit TDB using the JPL DE200 ephemeris[12] and the radio position J2000 $\alpha = 08$ h 35 min 20.680 s, $\delta = -45°10'35.70''$ (J. H. Taylor, personal communication). The accuracy of the Rosat spacecraft clock is consistent to within ~0.5 ms over time intrvals of a few weeks, although over longer timescales there could be sytematic deviations as large as 4 ms. Owing to this long-term clock drift, we period-folded the photon times using the PSR0833−45 radio ephemeris (J. H. Taylor, personal communication) for the April and December data sets separately. Table 1 summarizes the radio ephemeris parameters used. Throughout the observations, the arrival times of the radio pulses were known to an accuracy better than one milliperiod. Consequently, there was no need for any period search; each X-ray photon could be directly phase-related to the radio. The resulting phase plots are shown in Fig. 1*a* and *b*, where phase 0 is the radio phase accurate to ±0.05.

We evaluated the significance of the pulsations with the Z_n^2 test[13]. The main advantage of this test is that it is independent of binning, and the increase of Z_n^2 as a function of n, the number of summed harmonics, shows the harmonic content of the pulse shape. For both April and December observations, the signal increased up to 3 harmonics to Z_3^2 values of 31.2 and 50.1 respectively. Considering that for uniformly distributed phases the values of Z_3^2 should be distributed like χ^2 with 6 degrees of freedom, the probability of random occurrence for the April observation is 2.3×10^{-5} and for December 4.5×10^{-9}. The signal disappears as we change the period of folding or the direction of the accepted events from those expected. We conclude that in both data sets there is strong evidence for pulsations. On the other hand, the two pulse shapes appear different and out of phase. We checked the consistency of the two data sets being drawn from the same parent distribution with a χ^2 test as we varied the phase delay between the two. The results indicate that the two sets are compatible (at the 90% confidence level) if the December data had an additional positive offset of 4–13 ms. Considering that the long-term absolute Rosat time determination could easily have an error of ±2 ms, we think it likely that we are seeing the effect of timing errors rather than real changes in pulse shape or phase. The fraction of the counts

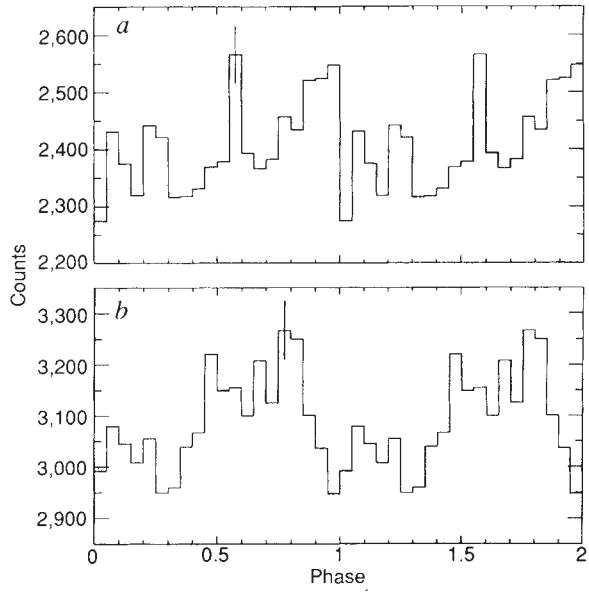

FIG. 1 Folded light curves of the Vela pulsar photons in the energy range 0.06 to 2.4 keV for (*a*) the April 1991 data set, (*b*) the December 1991 data set. Phase 0 and 1 refer to the radio pulse with an estimated accuracy of ±0.05.

TABLE 1 Radio pulsar data used in pulsation analysis

Date	Epoch* (TDB JD)	ν_0 (Hz)	$\dot{\nu}$ (Hz s^{-1})
1991 April 22.0–23.9	2448369.821485628	11.198852134351	-1.557662×10^{-11}
1991 December 4.7–19.8	2448604.913344683	11.198564513900	-1.565618×10^{-11}

* The epoch is also the radio arrival time at the Solar System barycentre.

that are pulsed in Fig. 1*b* is $4.4\pm1.1\%$, which is consistent with the upper limit of ~9% for broad pulse shapes established by the Einstein observatory[6]. The general features of the soft X-ray light curve of the Vela pulsar include a smaller pulse in the phase range 0.0–0.3 and a larger double-peaked pulse in the phase range 0.4–1.0. The X-ray pulse is complex and does not match the shapes of the γ-ray, optical or radio pulse. Compared with the radio phase, the bulk of the X-ray pulse resides in the phase region 0.5–1.0 whereas the optical and the γ-ray pulse dominate the region 0.1–0.6 (ref. 4). We should point out that this is the first attempt at absolute phase comparisons with the Rosat data. There is still concern that the calibration of the spacecraft clock may contain an offset (P. Predehl, personal communication).

To investigate the spectral characteristics of the pulses, the point source and the compact nebula, we first had to determine the contributions from each component as a function of radius and energy. To this end, we constructed a maximum likelihood procedure in which we fitted the observed radial count density profiles out to 3′ in 24 energy bins (covering channels 6–240) with the following parameters: (1) the counts $N_{ps}(E)$ from the point source distributed with the point response function of Rosat at that energy; (2) the counts $N_{di}(E)$ from the compact nebula distributed with various radial nebular distribution functions determined iteratively; (3) a flat background count density BG(E). The results of the fits were satisfactory and yielded the raw count distribution as a function of Rosat energy channel for the point-like and diffuse components separately (Fig. 2). The point-source spectrum is softer than the nebular component. The scale size of the nebula is compatible with the high-angular-resolution Einstein High-Resolution-Imager data[6] and the Exosat Channel Multiplier Array data[7]. The soft point-source spectrum is supported by the earlier Exosat filter spectroscopy results[7]. Using these energy-dependent functions, we estimate that the pulsed fraction of the point-source counts is 11%. With this data set we also did spectral fits to the compact nebula and the point source. The compact nebula is well fitted by either a power-law or thermal bremsstrahlung spectrum; we get unacceptable fits to a black-body spectrum. For the point source, we fitted the data with black-body and power-law models, which give acceptable results. We also fitted this data below 1.2 keV to eliminate the high energy tail. These results are summarized in Table 2. Finally, we did spectral fits to the pulsed counts in five energy channels with sufficient statistical significance. As in the raw spectrum of the point source, there were no pulsed counts above 1.2 keV, again confirming that the pulsed photons were soft. The spectrum best fitting the pulsed photons was a black-body model with parameters similar to the point source. These results are included in Table 3. Again the pulsed bolometric luminosity comes out to be ~10% of the bolometric luminosity of the point source. It is also reassuring that the spectral parameters of the pulsed photons, chosen on the basis of time variation, are almost identical to the point-source photons chosen on the basis of radial count-density fits.

The period (~0.089 s) and period derivative of the Vela pulsar yield a characteristic age $\tau\approx11{,}000$ yr and a rotational energy loss rate $\dot{E}\approx7\times10^{36}$ erg s^{-1} (ref. 14). Among the five previously known pulsars that emit pulsed X-rays, the age of the Vela pulsar lies between the young, ~10^3-yr ages of the Crab pulsar, PSR0540−69 and PSR1509−58 and the old, ~10^5-yr ages of PSR0656+14 and Geminga[15]. The young pulsars all have a power-law-type spectrum which is interpreted as the magnetospheric emission of the relativistic electrons and positrons[16,17]. The older pulsars have a soft, black-body-like spectrum with some residual excess at higher energies[18,19]. Our results show that in X-rays, the Vela pulsar is similar to the older pulsars although it is a factor of 10 younger. The X-ray pulsed fraction of Vela (11%) is also comparable to those of PSR0656+14 (14%; ref. 18) and Geminga (15%; ref. 19). The combination of parameters that determine the transition of the X-ray spectrum from the hard magnetospheric emission to the soft black-body-like emission must have already exceeded the boundary for the Vela pulsar. Black-body fits to the spectrum of the Vela point source give surface temperatures in the range $1.5\text{–}1.6\times10^6$ K, which is compatible with some cooling models and reheating processes[20–22], but the observed luminosities of $4\text{–}5\times10^{32}$ erg s^{-1} imply that the radius of the Vela pulsar is only 3–4 km rather than the expected 10–18 km (at infinity). This discrepancy can be resolved when we take into account the spectral modification of the neutron star atmosphere, including the effect of strong magnetic fields[18,23–25]. The lower luminosity and similar temperature of the black-body fits to the pulsed flux suggest a radius around three times less for the origin of this component. The high harmonic content of the pulse shape would require a complex surface temperature structure or angle-dependent opacities due to the magnetic field geometry.

The power-law fit to the compact nebula is consistent with the Einstein IPC results[6], although the IPC fit includes both the compact nebula and the point source together. The factors determining the size of this distinct region are still not clear[7]. Its luminosity must derive from the wind of the pulsar, but the fact that the luminosity of the compact nebula is only $\sim3\times10^{-4}$ of the spin-down luminosity implies that this region is

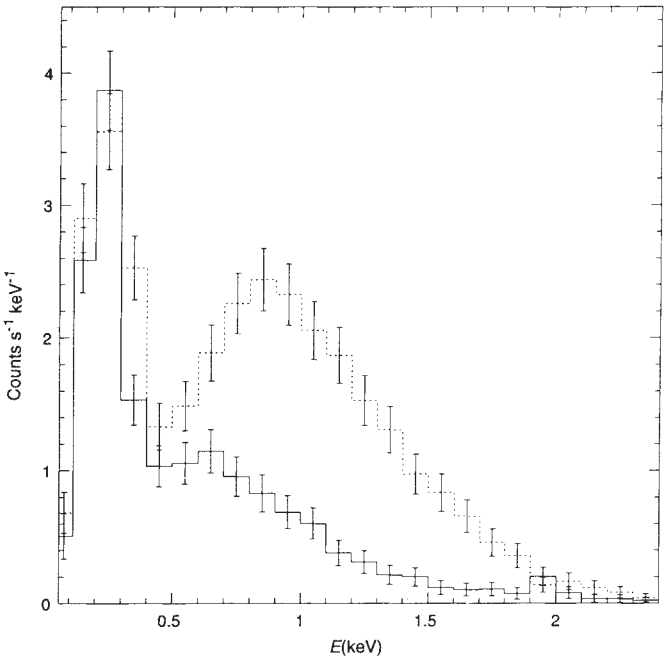

FIG. 2 Energy distribution of the point source (solid lines) and the compact nebula photons (dashed lines) as derived from the energy-dependent radial-count-density distributions. The errors are estimated from the range of acceptable radial-count-density models of the compact nebula.

TABLE 2 Spectral models and fit parameters

Model	N_H (10^{20} cm^{-2})	Model parameter	L_x^* (10^{32} erg s^{-1})
Compact nebula (0.06–2.4 keV)			
Thermal brems.	2.0 ± 0.5	$kT = 1.6 \pm 0.2$ keV	14
Power-law	3.0 ± 0.5	photon index = −2.0 ± 0.2	18
Point source (0.06–2.4 keV)			
Black-body	0.5 ± 0.4	$kT = 0.15 \pm 0.01$ keV	4.3
Power-law	4.3 ± 1.0	photon index = −3.3 ± 0.4	26
Point source (0.06–1.2 keV)			
Black-body	0.9 ± 0.6	$kT = 0.13 \pm 0.02$ keV	4.8
Power-law	4.4 ± 1.5	photon index = −3.3 ± 0.8	26
Pulsed photons (0.06–2.4 keV)			
Black body	1.0 ± 0.8	$kT = 0.14 \pm 0.02$ keV	0.5

* The luminosity at 500 pc in the energy band 0.1–2.4 keV. For black-body fits it is the bolometric luminosity.

remarkably transparent to the low-frequency dipole waves and the relativistic hydromagnetic wind generated at the magnetosphere of the pulsar.

This detection of the Vela pulsar, together with the recent Rosat discoveries of Geminga[15] and PSR0656+14 (ref. 18) as pulsed soft X-ray sources, implies that Rosat can study the X-ray spectrum and pulse profiles of 10^4–10^5-yr-old neutron stars within a few kiloparsecs from us. Other such discoveries together with observations at other wavelengths may allow us to construct a consistent picture of magnetospheric emission and the cooling properties of neutron stars. □

Received 21 October; accepted 23 November 1992.

1. Large, M. I., Vaughan, A. E. & Mills, B. Y. *Nature* **220,** 340–341 (1968).
2. Wallace, P. T. *et al. Nature* **266,** 692–694 (1977).
3. Thompson, D. J., Fichtel, C. E., Kniffen, D. A. & Ögelman, H. B. *Astrophys. J.* **214,** L17–L18 (1977).
4. Kanbach, G. *et al. Astr. Astrophys.* **90,** 163–169 (1980).
5. Tümer, O. T. *et al. Nature* **310,** 214–216 (1984).
6. Harnden, F. R. Jr, Grant, P. D. & Seward, F. D. *Astrophys. J.* **299,** 828–838 (1985).
7. Ögelman, H. & Zimmermann, H.-U. *Astr. Astrophys.* **214,** 179–185 (1989).
8. Harnden, F. R. Jr, Johnson, W. N. III & Haynes, R. C. *Astrophys. J.* **172,** L91–L94 (1972).
9. Harnden, F. R. Jr & Gorenstein, P. *Nature* **241,** 107–108 (1973).
10. Knight, F. K., Matteson, J. L., Peterson, L. E. & Rothschild, R. E. *Astrophys. J.* **260,** 553–560 (1982).
11. Trümper, J. *et al. Adv. Space Res.* **2,** 241–249 (1983).
12. Standish, M. *Astr. Astrophys.* **114,** 297–302 (1982).
13. Buccheri, R. *et al. Astr. Astrophys.* **128,** 245–251 (1983).
14. Manchester, R. N. & Taylor, J. H. *Astr. J.* **86,** 1953–1973 (1981).
15. Ögelman, H. in *Proc. Workshop Physics of Isolated Pulsars* (Cambridge Univ. Press, Cambridge, in the press).
16. Cheng, K. S., Ho, C. & Ruderman, M. *Astrophys. J.* **300,** 522–539 (1986).
17. Harding, A. K. *Astrophys. J.* **245,** 267–273 (1981).
18. Finley, J. P., Ögelman, H. & Kiziloğlu, Ü. *Astrophys. J.* **394,** L21–L24 (1992).
19. Halpern, J. P. & Holt, S. S. *Nature* **357,** 222–224 (1992).
20. Nomoto, K. & Tsuruta, S. *Astrophys. J.* **312,** 711–726 (1987).
21. Shibazaki, N. & Lamb, F. K. *Astrophys. J.* **346,** 808–822 (1989).
22. Page, D. & Applegate, J. H. *Astrophys. J.* **394,** L17–L20 (1992).
23. Romani, R. W. *Astrophys. J.* **313,** 718–726 (1987).
24. Miller, M. C. in *Proc. Workshop Physics of Isolated Pulsars* (Cambridge Univ. Press, Cambridge, in the press).
25. Ventura, J., Shibanov, Yu. A., Zavlin, V. E. & Pavlov, G. G. in *Proc. Workshop Physics of Isolated Pulsars* (Cambridge Univ. Press, Cambridge, 1992).

ACKNOWLEDGEMENTS. We thank Günther Hasinger for the time-corrected Rosat data. This work was supported by NASA LTSA Research Program.

Photoinduced electron transport across a lipid bilayer mediated by C_{70}

Kuo Chu Hwang & David Mauzerall

Rockefeller University, 1230 York Avenue, New York, New York 10021, USA

ELECTRON transport across a membrane is central to photosynthesis, to mitochondrial respiration and to the design of molecular systems for solar energy conversion. Relatively few synthetic molecules, however, have been shown to facilitate transport of electrons across a lipid bilayer[1–3]. We report here that C_{70} can act as both a photosensitizer for electron transfer from a donor molecule and a mediator for electron transport across a lipid bilayer membrane. The steady-state photocurrent density obtained from the C_{70}–bilayer system is about 40 times higher, at comparable light intensities, than that of the carotene–porphyrin–quinone system[2], previously the most efficient artificial system. The C_{70}–bilayer system has a quantum yield of about 0.04, while the stability (tens of minutes) and turnover number (electrons transported per C_{70} before decay) of 10^3 are one to three orders of magnitude greater than those of other systems[1–3]. We anticipate that other higher fullerenes may also provide the basis for efficient transmembrane electron-transport systems.

C_{60} has been shown[4–6] to be a good electron acceptor when photoexcited. Cast films of C_{60} on metal electrode surfaces have been found to act as an *n*-type semiconductor, but the dark current is at least an order of magnitude larger than the photocurrent[7]. Polyvinyl carbazole doped with C_{60} is an efficient photoconductor, in which holes in the carbazole valence band act as the charge carriers and the C_{60} molecules act as the photoactive electron acceptors[8]. We have reported elsewhere[9] that both C_{60} and C_{70} embedded within a lipid membrane can act as efficient electron acceptors from photoexcited amphoteric zinc porphyrin absorbed to the membrane; the fullerene anions carry the charges deeply into the bilayer, enhancing the photovoltage. We show here that these fullerenes can transpose electrons completely across the membrane.

Figure 1*a* shows a transmembrane photocurrent of 4 nA produced by continuous illumination of a lipid bilayer containing C_{70} which separates two aqueous compartments with ascorbate and sodium anthraquinone 2-sulphonate (hereafter, ascorbate |C_{70}| AQS, where | | represents the two membrane–water interfaces). The sign of the photovoltage[9] and of the photocurrent together with redox potentials (see below) show that electrons are transported from aqueous ascorbate to photoexcited C_{70} in the membrane, then to AQS in the other aqueous interface. The redox potentials are as follows: $E^0_{\text{ascorbate(ox)/ascorbate(red)}} = -0.21\ V_{SCE}$ (ref. 10), $E^0_{C_{70}/C_{70}^-} = -0.43\ V_{SCE}$ (ref. 11), $E^0_{^3C_{70}/C_{70}^-} = \sim +1.14\ V_{SCE}$ (ref. 5) (the first reduction potential[11] and the triplet energy[12,13] of C_{60} and C_{70} are about the same). The presence of molecular oxygen suppresses >95% of the photocurrent. Our photovoltage measurements[9] indicate that interfacial electron transfer from (60 mM) ascorbate to (0.8 mM) C_{70} occurs on a timescale of ~80 μs. The lifetime of photoexcited C_{70} is 0.67 ns (ref. 14) for the singlet state and 51 ms (ref. 12) for the triplet state, so triplet C_{70} must be the reactive species. No photocurrent (<0.1 pA) was observed whenever C_{70} was omitted from the bilayer, proving that C_{70} is the transmembrane electron carrier. On long irradiation (30 min, Fig. 1*b*), the photocurrent began to decay after ~2 min, and the decay rate increased with increasing light intensity. The photocurrent remains at its final low level after 30 min in the dark. The cause of the slow photocurrent decay is currently unclear. The total charge transported by C_{70} across the bilayer is 4 μC (or 2.5×10^{13} electrons). We estimate that there are $\leq 4 \times 10^{10}$ molecules of C_{70} in the bilayer, assuming the ratio of C_{70} to lipid remains constant from the decane–toluene solution to the bilayer. The turnover number of the system (one electron per C_{70}) is thus ~10^3.

When a membrane is permeable to electrons, a Nernst potential is generated by the redox potential difference of a redox pair in the two aqueous compartments[1,15]. As shown in Fig. 2, on irradiation the observed potential of the C_{70}-containing membrane is proportional to the calculated Nernst potential difference created by the $[\text{ascorbate}]_{red}/[\text{ascorbate}]_{ox}$ redox pair, with a slope of 0.72. In contrast, a small, constant (−1 ± 1 mV)